Coversheet for "Climate forcing insufficient to explain sea-level lowstands in Maldives during Common Era"

Christopher G. Piecuch[1,†], Andrew C. Kemp[2,‡], & Geoffrey Gebbie[1,*]

[1]*Department of Physical Oceanography, Woods Hole Oceanographic Institution, Woods Hole, Massachusetts, USA*

[2]*Department of Earth and Ocean Sciences, Tufts University, Medford, Massachusetts, USA*

† cpiecuch@whoi.edu

‡ andrew.kemp@tufts.edu

* jgebbie@whoi.edu

Climate forcing insufficient to explain sea-level lowstands in Maldives during Common Era

Christopher G. Piecuch[1], Andrew C. Kemp[2], & Geoffrey Gebbie[1]

[1]*Department of Physical Oceanography, Woods Hole Oceanographic Institution, Woods Hole,*

Massachusetts, USA

[2]*Department of Earth and Ocean Sciences, Tufts University, Medford, Massachusetts, USA*

Reconstructions of Common-Era sea level are informative of relationships between sea level and natural climate variation, and the uniqueness of modern sea-level rise[1]. Kench et al.[2] recently reconstructed Common-Era sea level in the Maldives, Indian Ocean, using coral microatolls. They identified periods of 150–500 yr when sea level fell and rose at average rates of 2.7–4.3 mm yr^{-1}. These periods coincided with intervals of cooling and warming inferred from proxy reconstructions of sea-surface temperature (SST) and radiative forcing (ref. 2, Fig. 2). Kench et al.[2] reasoned that these 0.8–0.9-m centennial-scale sea-level fluctuations were driven by climate, specifically thermal contraction and expansion of seawater. In contrast to previous studies[3,4], Kench et al.[2] argued that modern rates and magnitudes of sea-level rise caused by climate change have precedent during the Common Era. We use principles of sea-level physics to argue that pre-industrial radiative forcing and SST changes were insufficient to cause thermosteric sea-level (TSL) trends as large as reported for the Maldives[2].

Radiative forcing (e.g., related to solar activity[5] and volcanic eruptions[6]) varies over a broad

1

range of time scales, and influences global climate and sea level[7,8]. For example, models show that major volcanic eruptions during the twentieth century drove rapid interannual falls in global-mean sea level (order mm yr^{-1}) that were followed by gradual decadal rises (order tenths of mm yr^{-1}) as the climate system recovered[7]. To determine whether variability in radiative forcing on centennial and longer time scales in the Common Era was sufficient to drive TSL trends as large and sustained as those inferred for the Maldives[2], we express trends in TSL in terms of their equivalent net surface heat flux (see Supplementary Information). Using a thermal expansion coefficient characteristic of tropical surface ocean waters (3.1–3.4×10^{-4} °C^{-1}), we estimate that a net flux of 1.0–1.8 W m^{-2} is required for a TSL trend of 2.7–4.3 mm yr^{-1}. The required flux is stronger than centennial-scale variations in reconstructions of radiative forcing[5,6], which can be uncertain, but exhibit magnitudes < 0.4 and < 0.2 W m^{-2} over time scales of 150 and 500 yr, respectively (95% confidence; Fig. 1a; Supplementary Information). In other words, radiative forcing likely accounts for $< 31\%$ ($< 18\%$) of the forcing required to produce 150-yr (500-yr) TSL trends of 2.7–4.3 mm yr^{-1} (Fig. 1c, purple). This required net heat flux is also larger than the rate of contemporary global upper-ocean warming since 2005 CE (0.5–0.7 W m^{-2}) estimated from profiling-float observations[9].

We also estimate what SST trend is required to generate a given trend in TSL (Supplementary Information). We assume that magnitudes of ocean temperature changes decay exponentially from the surface to the bottom over an e-folding depth scale of 750–1250 m. This translates to 45–61% (83–94%) of ocean heat storage occurring in the upper 700 m (2000 m), similar to estimates from model-data syntheses[10,11] of changes in global ocean heat content over the past 140–270 yr. Using a reasonable global-ocean, volume-averaged thermal expansion coefficient (1.6–1.9×10^{-4} °C^{-1}),

2

41 we find that TSL trends of 2.7–4.3 mm yr^{-1} require attendant SST trends of 1.2–3.6 °C century^{-1}

42 (Fig. 1b). This estimate is supported by long integrations of an empirical ocean circulation model[12],

43 which suggest that TSL trends of 2.7–4.3 mm yr^{-1} sustained for 150 and 500 yr require SST trends

44 of 1.8–2.9 and 0.9–1.4 °C century^{-1}, respectively (Fig. 1b; Supplementary Information). These

45 model results are consistent with the basic expectation that, on longer time scales under sustained

46 climate forcing, relatively more heat penetrates the deep ocean, requiring a comparatively smaller

47 SST change to produce a given TSL trend.

48   The required SST trends are larger than inferences from 10 reconstructions of Common-Era

49 SST[13] in the Indian Ocean and Indonesian Throughflow, which show trends of < 0.8 and < 0.2 °C

50 century^{-1} on time scales of 150 and 500 yr, respectively (95% confidence; Fig. 1b; Supplementary

51 Information). Although they are not from the Maldives, these SST reconstructions are informative

52 of the range of centennial SST trends over the tropical Indian Ocean during the Common Era. We

53 find that SST reconstructions likely account for $< 37\%$ and $< 7\%$ of the temperature trends needed

54 to explain TSL trends of 2.7–4.3 mm yr^{-1} on time scales of 150 and 500 yr, respectively, assuming

55 exponential vertical structure (Fig. 1c, blue). Instead using the empirical ocean circulation model,

56 we estimate corresponding percentages of $< 33\%$ and $< 13\%$ (Fig. 1c, orange). Even making the

57 extreme assumption that ocean temperature trends are vertically uniform, which is unrealistic given

58 the long adjustment time scales in the deep ocean[12], we find that SST trends required for trends in

59 TSL of 2.7–4.3 mm yr^{-1} (Fig. 1b) are generally larger than are inferred from SST reconstructions,

60 especially for periods > 300 yr (Fig. 1c, green).

3

Kench et al.[2] reconstructed a sea-level trend of 4.2 mm yr^{-1} in the Maldives for the modern industrial interval between 1807 and 2018 CE. Comparable trends of 3.2–4.7 mm yr^{-1} are seen in 2 tide-gauge sea-level records[14] in the Maldives for the past 25–30 yr (Supplementary Information Table S1). However, smaller sea-level trends of 0.6–1.5 mm yr^{-1} are seen for the past 80–140 yr in 4 long tide-gauge records available along coastal India (Supplementary Information Table S1). This underscores that sea-level trends are time-scale dependent, and can be influenced by stochastic processes that tend to decrease in magnitude with increasing time scale. Moreover, the Indian tide gauges show good correlation with, and similar trends to, the tide gauges from the Maldives for the overlapping interval since ~ 1990 CE (Fig. 1d; Supplementary Information Table S1). This means that the tide gauges in India are informative of sea-level variability more broadly across the region through time. Thus, the average rate of sea-level rise since 1807 CE reconstructed by Kench et al.[2] in the Maldives from coral microatolls is faster than the quasi-centennial rates measured by nearby tide gauges, and is too large to be understood in terms of large-scale climate alone.

The sea-level reconstruction from the Maldives published by Kench et al.[2] adds to a growing atlas of Common-Era sea-level records[4] and provides a valuable constraint from a data-poor region. Our analyses suggest that the 0.8–0.9-m centennial sea-level variations in the Maldives are too large to have resulted from the thermal contraction and expansion of seawater due to large-scale climate forcing alone. Our results quantify how exceptional ocean cooling and warming near the Maldives would have been in a larger context were they sufficient to drive centennial sea-level trends as large as those determined by Kench et al.[2]. As Kench et al.[2] acknowledged, it is also unlikely that these centennial sea-level changes reflect ice and water mass redistribution[15] as similar contemporaneous

sea-level changes are absent from other intermediate- and far-field reconstructions of Common-Era

sea level[3,4]. Thus, we hypothesize that sea-level changes reported by Kench et al.[2] resulted mainly

from local-scale processes unrelated to climate, and do not falsify the conclusion that modern rates

and magnitudes of centennial sea-level rise (since ~ 1800 CE) driven by climate are unprecedented

in the Common Era[3,4]. More proxy reconstructions from the Maldives and the wider tropical Indian

Ocean are necessary to evaluate our hypothesis and to more rigorously quantify local, regional, and

global effects on sea level.

References

1. Kemp, A. C. et al. Paleo constraints on future sea-level rise. *Curr. Clim. Change Rep.*, **1**, 205–215 (2015).

2. Kench, P. S. et al. Climate-forced sea-level lowstands in the Indian Ocean during the last two millennia. *Nat. Geosci.*, **13**, 61–64 (2020).

3. Kemp, A. C. et al. Climate related sea-level variations over the past two millennia. *P. Natl. Acad. Sci. U.S.A.*, **108**(27), 11017–11022 (2011).

4. Kopp, R. E. et al. Temperature-driven global sea-level variability in the Common Era. *P. Natl. Acad. Sci. U.S.A.*, **113**(11), E1434–E1441 (2016).

5. Steinhilber, F. et al. Total solar irradiance during the Holocene. *Geophys. Res. Lett.*, **36**, L19704 (2009).

6. Sigl, M. et al. Timing and climate forcing of volcanic eruptions for the past 2,500 years. *Nature*, **523**, 543–549 (2015).

7. Church, J. A. et al. Significant decadal-scale impact of volcanic eruptions on sea level and ocean heat content. *Nature*, **438**, 74–77 (2005).

8. Gleckler, P. J. et al. Krakatoa lives: The effect of volcanic eruptions on ocean heat content and thermal expansion. *Geophys. Res. Lett.*, **33**, L17702 (2006).

9. Cheng, L. et al. How fast are the oceans warming? *Science*, **363**, 128–129 (2019).

10. Zanna, L., et al. Global reconstruction of historical ocean heat storage and transport. *P. Natl. Acad. Sci. U.S.A.*, **116**(4), 1126–1131 (2019).

11. Gebbie, G., & Huybers, P. The Little Ice Age and 20th-century deep Pacific cooling. *Science*, **363**, 70–74 (2019).

12. Gebbie, G., & Huybers, P. The mean age of ocean waters inferred from radiocarbon observations: sensitivity to surface sources and accounting for mixing histories. *J. Phys. Oceanogr.*, **42**, 291–305 (2012).

13. Emile-Geay, J. et al. A global multiproxy database for temperature reconstructions of the Common Era. *Sci. Data*, **4**, 170088 (2017).

14. Holgate, S. J. et al. New data systems and products at the permanent service for mean sea level. *J. Coastal Res.*, **29**(3), 493–504 (2013).

15. Tamisiea, M. E., & Mitrovica, J. X. The moving boundaries of sea level change: understanding the origins of geographic variability. *Oceanography*, **24**(2), 24–39 (2011).

Author Contributions   All of the authors conceived of the study, designed the methods, and analyzed the data. CGP wrote the manuscript with input from ACK and GG.
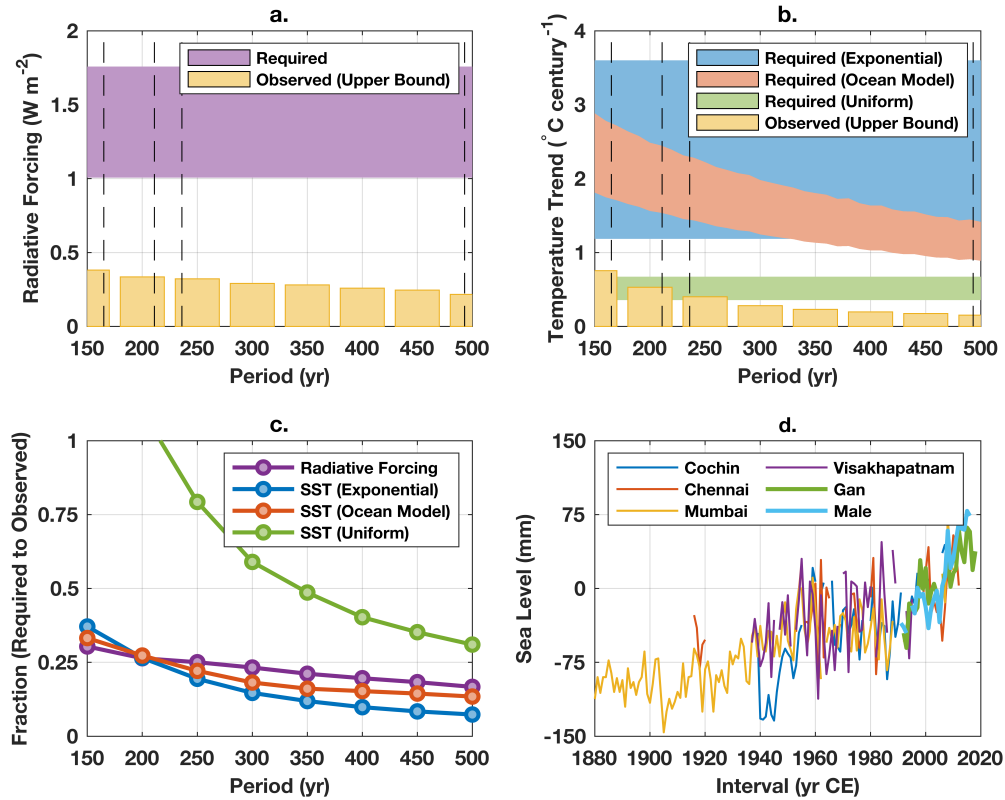
Data Availability   Temperature-sensitive Common-Era proxy records from the PAGES2k project[13] were taken from the current data version available from the National Climatic Data Center website on 22 Jan 2020 (`www1.ncdc.noaa.gov/pub/data/paleo/pages2k/pages2k-temperature-v2-2017/`). Only low-resolution oceanic data ("O2kLR") covering most of the Common Era in the study area were used. Numerical codes for the circulation model from Gebbie and Huybers[12] are available for download from GG's website (`https://www2.whoi.edu/staff/ggebbie/`). Total solar irradiance during the Holocene from Steinhilber et al.[5] was downloaded from the National Climatic Data Center FTP server on 3 Feb 2020 (`ftp.ncdc.noaa.gov/pub/data/paleo/climate_forcing/solar_variability/`). The estimates of volcanic aerosol forcing from Sigl et al.[6] are as provided in the online version of the paper as

7

141

Figure 1. a, Net surface heat flux required to generate a trend in thermosteric sea level (TSL) of

2.7–4.3 mm yr^{-1} (purple shading) exceeds the radiative-forcing magnitudes that likely took place

during 0–1800 CE on time scales of 150–500 yr (yellow bars; see Supplementary Information).

Dashed vertical black lines indicate the duration of sea-level trends reconstructed by Kench et al.[2]

for the Maldives (corresponding to −91 to 401, 552 to 717, 1521 to 1757, and 1807 to 2018 CE).

b, Sea-surface-temperature (SST) trends needed to generate a trend in TSL of 2.7–4.3 mm yr^{-1} for

8

150–500 yr based on the assumption that ocean temperature trends decay exponentially with ocean depth (blue shading) and from an empirical ocean circulation model[12] (orange shading) exceed the SST trends that likely took place during 0–1800 CE on time scales of 150–500 yr (yellow bars; see Supplementary Information). Only in the unrealistic case of assumed vertically uniform ocean heat storage do the SST trends needed for TSL trends of 2.7–4.3 mm yr^{-1} (green shading) overlap with the likely proxy-observed values, and then only for periods < 300 yr. Dashed vertical black lines are as in **a**. **c,** Radiative-forcing magnitudes and SST trends that took place over 0–1800 CE on time scales of 150–500 yr likely represent only a fraction (vertical axis) of the changes needed to produce TSL trends of 2.7–4.3 mm yr^{-1} (Supplementary Information). **d,** Tide-gauge sea-level records[14] from India (Cochin, Chennai, Mumbai, Visakhapatnam) are correlated with data records from the Maldives (Gan, Male) for the overlapping interval since ~ 1990. The records from India show longterm trends of 0.6–1.5 mm yr^{-1}, which is smaller than the value of 4.2 mm yr^{-1} reported by Kench et al.[2] for the Maldives between 1807–2018 CE using coral microatolls. Tide-gauge time series are centered on their average value during 1990–2013 CE.

Supplementary Information

Calculation of equivalent surface heat flux Heat conservation and hydrostatic balance together

164 dictate that a net surface heat flux Q effects a change in thermosteric sea level (TSL) h_T following,

$$\dot{h_T} = \frac{\alpha}{c_p \rho_0} Q, \tag{1}$$

165 where dot is time derivative, α thermal expansion coefficient, c_p specific heat capacity of seawater,

166 and ρ_0 density of seawater. Rearranging to solve for Q gives,

$$Q = \frac{c_p \rho_0}{\alpha} \dot{h_T}. \tag{2}$$

167 Values of 1.0–1.8 W m^{-2} quoted in the main text and shown in Fig. 1a are minimum and maximum

168 values computed from Eq. (2) using $\dot{h_T} \in \{2.7, 4.3\}$ mm yr^{-1} and $\alpha \in \{3.1, 3.4\} \times 10^{-4}$ °C^{-1}.

169 We use representative values of $c_p = 4 \times 10^3$ J kg^{-1} °C^{-1} and $\rho_0 = 1 \times 10^3$ kg m^{-3}.

170   Note that this formulation is in terms of a *net* heat flux Q, and does not explicitly account

171 for any damping effects[16]. As such, Q values computed here should be interpreted as the *minimum*

172 radiative-forcing anomaly needed to generate a given TSL trend. In other words, ratios of observed

173 to required radiative forcing (purple curve in Fig. 1c; see below) are conservative in the sense that

174 they represent upper bounds.

175 **Calculation of centennial anomalies in radiative forcing based on proxies** To estimate radiative

176 forcing, we summed together the 40-yr running-mean total solar irradiance values from Steinhilber

177 et al.[5] (linearly interpolated onto a yearly spacing) and annual atmospheric aerosol loading owing to

178 volcanic eruptions determined by Sigl et al.[6] (zero values were imputed for years without volcanic

179 eruptions) and removed the time average over the interval 0–1800 CE (Supplementary Fig. S1a–c).

180 We computed running averages of the reconstructed radiative-forcing anomaly series for averaging

181 periods between 150 and 500 yr in 50-yr increments (Supplementary Fig. S1d). With each of these

182 running-average time series, we computed absolute values and evaluated the 95th percentile of the

183 resulting time-smoothed radiative-forcing anomaly magnitude record (Supplementary Fig. S1e–f).

184 These 95th percentiles (yellow bars in Fig. 1a) reflect upper bounds on the radiative forcing values

185 at a given time scale (i.e., 95% of values are smaller than this). Implicit in our analysis, following

186 ref. 2, is the assumption that this global forcing applies over the central equatorial Indian Ocean.

187   To quantify, in a relative sense, to what extent the reconstructed radiative-forcing anomalies

188 were sufficient to generate TSL trends as large as the trends inferred in the Maldives[2], we evaluated

189 the ratio of the reconstructed radiative-forcing anomaly as a function of time scale (Supplementary

190 Fig. S1e–f) to the required radiative forcing estimated using Equation 2 (purple shading in Fig. 1a,

191 assumed to be a uniform distribution) and took 95th percentiles, giving the purple values shown in

192 Fig. 1c (cf. discussion below related to a similar calculation for SST trends).

193 **Calculation of the implied sea-surface-temperature (SST) trend** Trends in TSL $\dot{h}_T$ are related

194 to ocean temperature trends $\dot{T}(z)$ according to,

$$\dot{h}_T = \int_{-H}^{0} \alpha \, \dot{T}(z) \, dz, \tag{3}$$

195 where z is the vertical coordinate (positive upwards) and H the ocean depth. In the scaling analysis,

196 we assumed that,

$$\dot{T}(z) = \dot{T}_0 \exp\left(z/H_T\right). \tag{4}$$

11

Integrating and rearranging, we obtain the analytical solution for $\dot{T}_0$, which is the SST trend,

$$\dot{T}_0 = \frac{\dot{h_T}}{\alpha H_T} \left[1 - \exp\left(-H/H_T \right) \right]^{-1}. \tag{5}$$

Values of 1.2–3.6 °C century^{-1} in the main text are the minimum and maximum values computed from Eq. (5) using $\dot{h_T} \in \{2.7, 4.3\}$ mm yr^{-1}, $\alpha \in \{1.6, 1.9\} \times 10^{-4}$ °C^{-1}, $H_T \in \{750, 1250\}$ m, and $H = 4 \times 10^3$ m (cf. blue shading in Fig. 1b).

Assuming instead that $\dot{T}$ is vertically uniform, Eq. (5) reduces to the simplified form,

$$\dot{T}_0 = \frac{\dot{h_T}}{\alpha H} \tag{6}$$

Evaluating this equation using the same parameter values, and taking the minimum and maximum, we obtain the green shading in Fig. 1b.

Choice of e-folding depth scale We chose a range of 750–1250 m for the e-folding scale H_T of ocean temperature changes. This choice was motivated by published estimates[10,11] of global-ocean heat storage during the past 140–270 yr. The reconstruction of Zanna et al.[10] suggests that $\sim 75\%$ of global ocean heat storage since 1871 occurred in the upper 700 m and $\sim 95\%$ in the top 2000 m (their Fig. 1a–1c). The model simulation of Gebbie and Huybers[11] calculated from equilibrium at 1750 CE shows that $\sim 50\%$ and $\sim 85\%$ of the ocean heat content changes occurred at depths above 700 and 2000 m, respectively (their Fig. 4b). Since the 140–270-yr time scales highlighted in these studies[10,11] are on the short end of the 150–500-yr range considered here[2], we selected 750–1250 m for the e-folding depth scale as conservative values that allow comparatively more heat to penetrate the deep ocean, requiring a smaller change in SST to achieve a given TSL trend.

Circulation model calculations We run the circulation model from Gebbie and Huybers[12] with idealized concentration (Dirichlet) boundary conditions. We perform 100 iterations of a $40,000$-yr simulation with randomized phasing of the boundary conditions. Surface boundary conditions are globally uniform and follow a frequency spectrum with a power law of -1.64 following Huybers and Curry[17]. We use the global Green's function (or transit-time distribution) to produce simulated time series, and results are similar if using four surface patches to account for climate hemispheric asymmetries. We consider non-overlapping intervals of between 150 and 500 yr (10-yr increments) and compute SST and TSL trends within the equatorial Indian Ocean near the Maldives ($4°$N $78°$E; 3750-m depth). For each trend window, we fit a first-order least-squares trend line to all TSL-SST trend pairs (Supplementary Fig. S2). The slope of this fit was taken as the SST change per unit change in TSL for a particular time scale. For example, we found that a trend of 1 mm yr^{-1} in TSL corresponds to a SST trend of 0.67 and 0.33 $°$C century^{-1} at respective time scales of 150 and 500 yr. Slopes are multiplied by 2.7–4.3 mm yr^{-1} to produce the orange-shaded region in Fig. 1b.

Calculation of centennial SST trends from temperature-sensitive proxy data We analyzed all Common-Era SST proxy reconstructions from the PAGES2k consortium[13] from the Indian Ocean and around the Indonesian Throughflow (see Data Availability). This dataset comprises one record each from the Arabian Sea, Horn of Africa, southwest coast of India, the Philippines, South China Sea, and western equatorial Pacific, and four in Makassar Strait (Supplementary Figs. S3, S4a–j). We linearly interpolated each available record onto a common yearly interval, and then computed trends from each record for every 150- to 500-yr period between 0–1800 CE. This procedure gave a separate time series with all possible trends across the ten proxy locations for each trend period

13

235 between 150 and 500 yr. With each period-specific trend time series, we removed the overall mean,

236 took absolute values, and then computed the 95th percentile of these anomalous trend magnitudes

237 (Supplementary Fig. S4k–l). These 95th percentiles (yellow bars in Fig. 1b) reflect upper bounds

238 on the proxy SST trends at a given time scale (i.e., 95% of trends are smaller than these values).

239   Note that these SST proxies are not from the Maldives and thus are not truly collocated with

240 the sea-level reconstruction from Kench et al.[2]. Our approach follows that of Kench et al.[2] in that

241 we use available SST proxy records from nearby locations to interpret the sea-level reconstruction

242 from the Maldives, where "nearby" is taken to mean "in the Indian Ocean or around the Indonesian

243 Throughflow." However, we consider more SST records than do Kench et al.[2], including a record

244 from the southwest coast of India, which is $< 1,000$ km from the sea-level reconstruction in the

245 Maldives (Supplementary Fig. S3). Our calculations should thus be interpreted as spanning a

246 plausible envelope of possible SST trends (as a function of time scale) across the tropical Indian

247 Ocean during the Common Era. We believe that the true Common-Era SST history in the Maldives

248 is within this realistic range. In other words, our results quantify how unusual the SST trends in

249 the Maldives would have been, within a larger regional context, to be large enough to drive the

250 sea-level trends inferred by Kench et al.[2].

251   As with radiative forcing, we quantified the relative extent to which reconstructed SST trends

252 were large enough to generate TSL trends as large as those in the sea-level reconstruction from the

253 Maldives[2]. We evaluated the ratio of the amplitudes of reconstructed SST trends (Supplementary

254 Fig. S4k–l) to the required SST trends using Equations 5 and 6 and from the empirical circulation

14

model[12] (blue, green, and orange shading in Fig. 1b, respectively, which we assumed were uniform distributions) and took the 95th percentiles as a function of time scale. This method produced the respective blue, green, and orange values in Fig. 1c.

Instrumental tide-gauge sea-level data To interpret the most recent (1807–2018 CE) sea-level trend for the Maldives from Kench et al.[2], we used tide-gauge annual-mean sea-level records from the Permanent Service for Mean Sea Level[14] (see Data Availability). We used all > 70-yr records in the database from coastal India (4 time series), and all records from the Maldives (2 time series). For all records, we computed best estimates of least-squares trends to the available data, ignoring data gaps. These trend values are given in Supplementary Table S1. Note that we do not consider the long (82-yr) tide-gauge record from Garden Reach, India, since it is located far upstream in the Bhāgirathi-Hooghly, near Kolkata, and is not reflective of large-scale, open-ocean conditions.
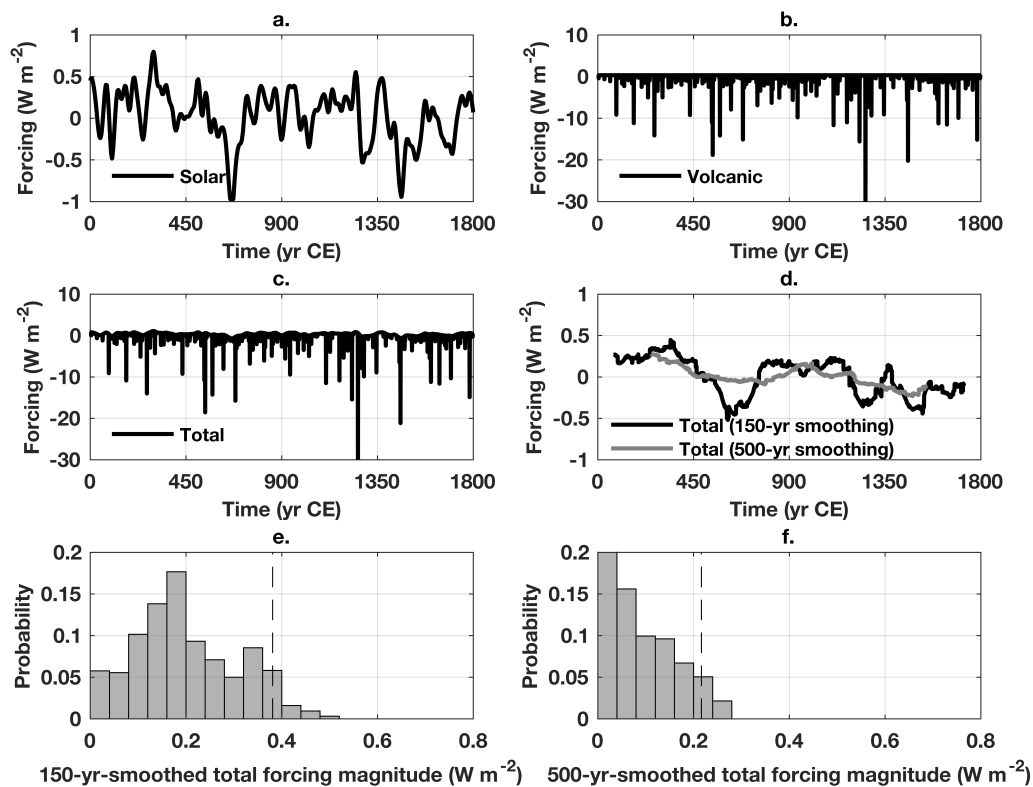
Additional References

16. Douglass, D. H. & Knox, R. S. Climate forcing by the volcanic eruption of Mount Pinatubo. *Geophys. Res. Lett.*, **32**, L05710 (2005).

17. Huybers, P. & Curry, W. Links between annual, Milankovitch and continuum temperature variability. *Nature*, **441**, 329–332 (2006).

18. Tierney, J. E. et al. Past and future rainfall in the Horn of Africa. *Sci. Adv.*, **1**(9), e1500682 (2015).

274   19. Doose-Rolinski, H. et al. High-resolution temperature and evaporation changes during the Late

275   Holocene in the northeastern Arabian Sea. *Paleoceanography*, **16**(4), 358–367 (2001).

276   20. Saraswat, R. et al. Deglaciation in the tropical Indian Ocean driven by interplay between the

277   regional monsoon and global teleconnection. *Earth Planet. Sc. Lett.*, **375**, 166–175 (2013).

278   21. Zhao, M. et al. A millennial-scale $U_{37}^{K'}$ sea-surface temperature record from the South China

279   Sea ($8°N$) over the last 150 kyr: Monsoon and sea-level influence. *Palaeogeogr. Palaeocl.*,

280   **236**(1–2), 39–55 (2006).

281   22. Linsley, B. K. et al. Holocene evolution of the Indonesian throughflow and the western Pacific

282   warm pool. *Nat. Geosci.*, **3**, 578–583 (2010).

283   23. Newton, A. et al. Changes in the Indonesian Throughflow during the past 2000 yr. *Geology*,

284   **39**(1), 63–66 (2011).

285   24. Oppo, D. W. et al. 2,000-year-long temperature and hydrology reconstructions from the Indo-

286   Pacific warm pool. *Nature*, **460**, 1113–1116 (2009).

287   25. Stott, L. et al. Southern Hemisphere and Deep-Sea Warming Led Deglacial Atmospheric CO_2

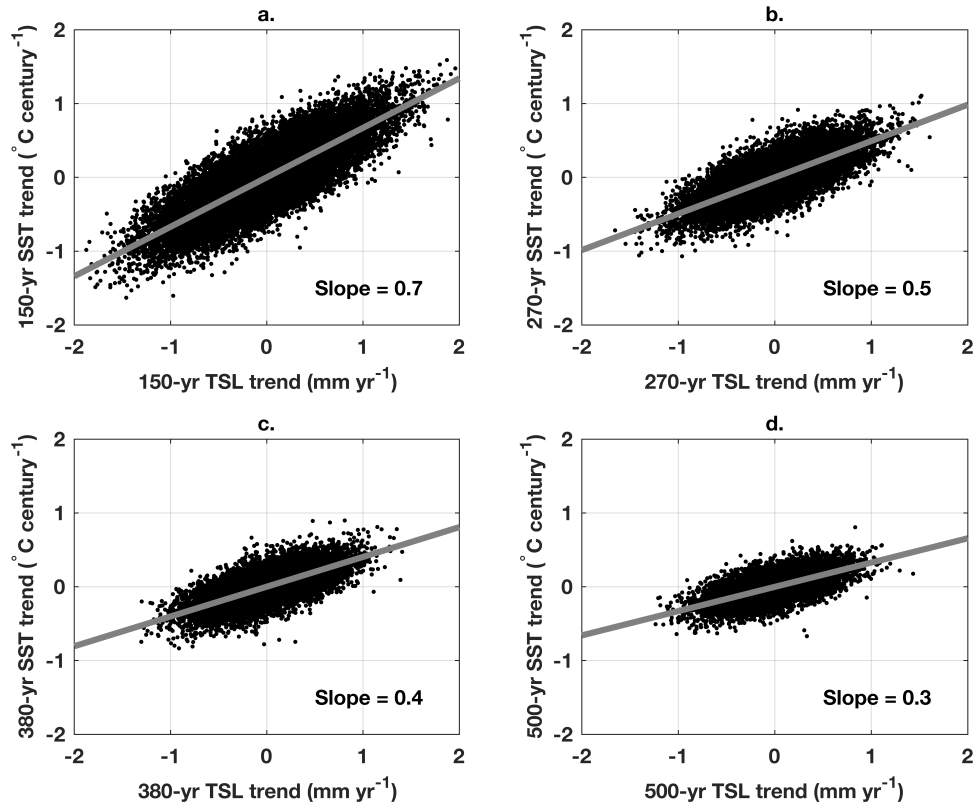288   Rise and Tropical Warming. *Science*, **318**(5849), 435–438 (2007).

Location	Lat (°N)	Lon (°E)	Trend (mm yr^{-1})	Length (yr)
Chennai, India	13	80	0.57 (1.87)	1916–2015
Visakhapatnam, India	18	83	0.92 (3.95)	1937–2013
Mumbai, India	19	73	0.84 (4.21)	1878–2015
Cochin, India	10	76	1.51 (3.23)	1939–2013
Gan, Maldives	−1	73	3.21	1989–2018
Male, Maldives	4	74	4.70	1991–2016

Supplementary Table S1. Names, locations, and record lengths of tide-gauge sea-level records used here. The trend is the best estimate of the slope of a least-squares linear fit to the available data (ignoring any data gaps). Parenthetical values for Indian tide gauges (Chennai, Visakhapatnam, Mumbai, Cochin) are trends since 1990 for direct comparison with the trends from the Maldivian gauges (Gan, Male).
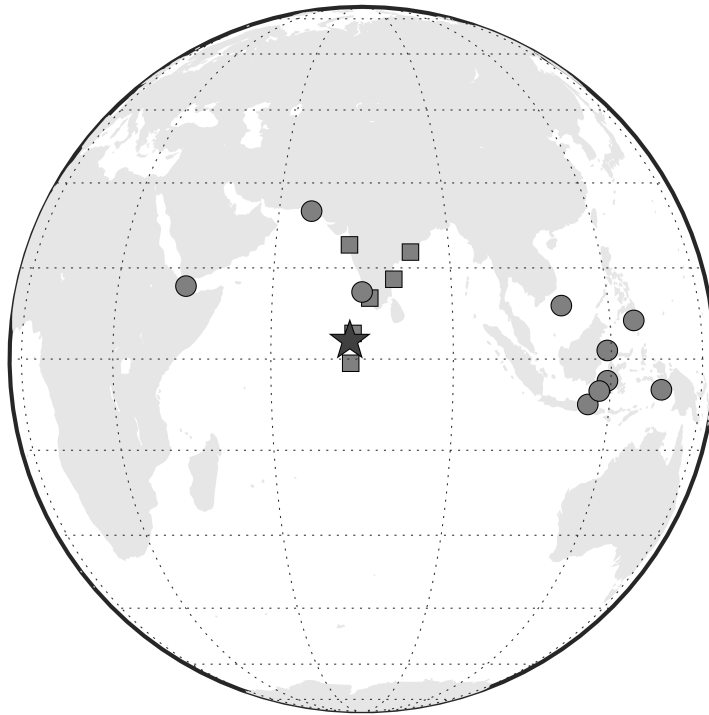
Supplementary Figure S1. a, Solar irradiance from Steinhilber et al.[5]. **b,** Volcanic aerosol forcing

from Sigl et al.[6]. **c,** Total radiative forcing (sum of time series from panels **a** and **b**). **d,** Smoothed

radiative forcing (time series from panel **c** with a 150- and 500-yr running-mean smoother applied).

Mean values during 0–1800 CE are removed from the time series in panels **a–d**. **e,** Histogram of

150-yr-smoothed forcing amplitudes from panel **d**. Black dashed vertical line is the 95th percentile.

f, As in **e** but for 500-yr-smoothed values.

18

296

Supplementary Figure S2. a, Black dots are all pairs of 150-yr TSL and SST trends from the long empirical circulation model integrations. Gray line is a trend line fit to the scatter, where the slope (indicated to the bottom right) is the change in SST trend per unit change in TSL trend in units of $(^{\circ}\mathrm{C}\ \mathrm{century}^{-1})\big/(\mathrm{mm}\ \mathrm{yr}^{-1})$. **b–d,** As in **a** but for periods of **b,** 270 yr, **c,** 380 yr, and **d,** 500 yr. Longer periods permit a more vertically homogeneous temperature response.
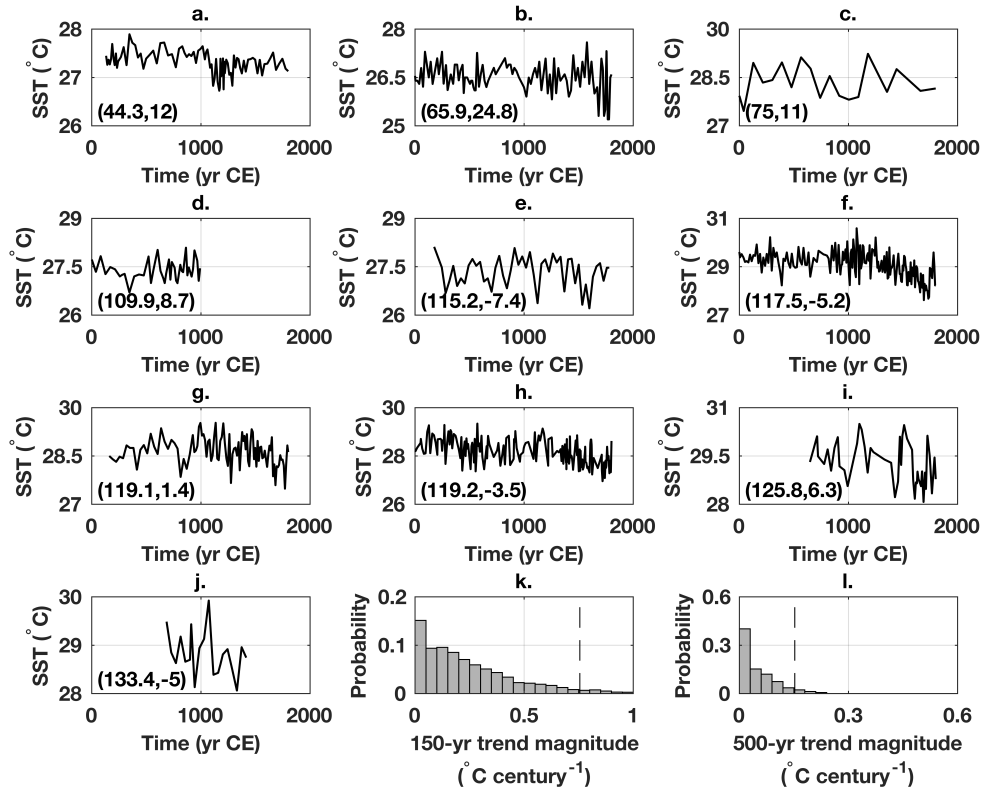
302

Supplementary Figure S3. Locations of proxy and instrumental data assets used in this study. Dark gray star is the location of the sea-level reconstruction from the Maldives. Light gray circles and squares are, respectively, are the locations of SST proxies and tide-gauge sea-level records.

Supplementary Figure S4. Common-Era proxy SST reconstructions from **a,** Horn of Africa[18], **b,** Arabian Sea[19], **c,** southwest coast of India[20], **d,** South China Sea[21], **e–h,** Makassar Strait[22–24], **i,** Philippines[25], and **j,** western equatorial Pacific[25]. Longitude (°E) and latitude (°N) are given in parenthesis at bottom left. Histograms of anomalous SST trend amplitudes across all ten sites for **k,** 150-yr and **l,** 500-yr periods. Black dashed vertical lines are 95th percentiles of the distributions.